Anion Effect in Electrochemical CO_2 Reduction: Enhanced Selectivity Enabled Through Anion Modulation

Ji Mun Yoo and Maria R. Lukatskaya*

Electrochemical Energy Systems Laboratory, Department of Mechanical and Process Engineering, ETH Zurich, 8092 Zurich, Switzerland

*mlukatskaya@ethz.ch

ABSTRACT:

Electrochemical CO_2 reduction reaction (eCO_2RR) offers a pathway to produce valuable chemical fuels from CO_2 molecules. However, its efficiency in aqueous electrolytes is hindered by the concurrent H_2 evolution reaction (HER), which takes place at similar potentials. While recent studies have highlighted critical role of cation selection to improve efficiency of eCO_2RR, targeted studies elucidating anion effect on eCO_2RR activity and selectivity are lacking. Herein, we present a systematic investigation of the anion-dependent eCO_2RR selectivity and activity on gold catalyst using *in situ* Differential Electrochemical Mass Spectrometry (DEMS) among wide range of anions. Our results reveal that by replacing bicarbonate with carboxylate anions, HER is largely suppressed. Furthermore, we show that propionate and acetate can promote eCO_2RR on par with bicarbonate, unlike other studied anions that display largely increased eCO_2RR overpotential. Notably, propionate benefits from both suppressed HER and eCO_2RR kinetics comparable to bicarbonate: reaching impressive Faradaic Efficiency close to 100% while displaying high CO production rates that are comparable to bicarbonate. These insights underscore the vital role of anion selection in achieving highly efficient eCO_2RR in aqueous electrolytes.

INTRODUCTION

The increasing concerns about environmental sustainability have driven intense research efforts for efficient technologies to convert CO_2, a greenhouse gas, into value-added chemicals and fuels.[1-2] Electrochemical CO_2 reduction reaction (eCO_2RR) has emerged as a promising approach, offering an avenue for sustainable carbon feedstock production using renewable electricity at ambient conditions.[3-5] However, eCO_2RR in aqueous electrolytes is characterized by reduced efficiency due to concomitant H_2 evolution reaction (HER) at the cathode surface that take place at similar potentials. Considering both reactions involve charge transfer at electrified catalyst surface and deprotonation of water molecules, selectivity between eCO_2RR and HER is largely determined by the local chemical environment at electrochemical interfaces, including double-layer speciation, local pH, electric field modulation, and mass transport within diffusion layer.[6-12] Therefore, to maximize CO_2 conversion efficiency, it is essential to reveal the role of each electrolyte specie during eCO_2RR (e.g. cations, anions and solvent molecules).

In this regard, current research efforts focus on formulating the design rules of electrolyte engineering for selective eCO_2RR.[8, 13-15] For example, recent studies have revealed the critical role of alkali cation presence,[16] identity (e.g. Li^+, Na^+, K^+, and Cs^+),[17-20] and concentration[21] in promotion of eCO_2RR selectivity. Cs^+ and K^+ show an

enhanced activity towards CO_2 reduction by effectively stabilizing the reaction intermediates (i.e., adsorbed CO_2^-) through either larger electric field[18] or stronger electrostatic interaction[16] compared to alkali cations with larger hydrated radius, such as Li^+ and Na^+. Also, HER-suppressing cationic effect was recently proposed by Qin et al. that interfacial cations induce lower HER kinetics by blocking HER active sites.[22]

In addition to the cation effect, the choice of anions can also play a crucial role in determining the eCO_2RR selectivity. However, current understanding of the anion effect remains limited. Bicarbonate (HCO_3^-) is widely employed as a benchmark anion in eCO_2RR studies.[23-26] Because of its chemical equilibrium with dissolved CO_2, bicarbonate is postulated to increase local CO_2 concentration at reactive electrochemical interface and, hence, enhance CO_2 reduction kinetics.[23-24] Moreover, due to its buffering effect, bicarbonate can suppress local pH increase near catalyst surface where hydroxide (OH^-) ions are generated during reduction reactions, thus alleviating the chemical depletion of dissolved CO_2 at a high reaction rate. Meanwhile, halide ions (e.g. Cl^-, Br^-, and I^-) are also reported to have a significant impact on the eCO_2RR selectivity.[27-29] As these ions exhibit strong adsorption on the metal surfaces,[27, 28] they can modulate the electronic structure of the active sites and facilitate/suppress specific reaction pathways.[29, 30] Moreover, strong adsorption of halide anion can be utilized to induce catalyst surface faceting through electrochemical roughening, leading to development of eCO_2RR-active crystal facets.[30, 31] Still, compared to the well-established cationic effect on eCO_2RR selectivity, the systematic investigation of the anion effect has been limited. The understanding of how different anions influence the eCO_2RR process is still elusive, hindering the development of effective electrolyte engineering design rules for achieving highly selective CO_2 conversion process. To address this, more anions should be systematically explored in terms of eCO_2RR activity and selectivity.

In this study, we probe and compare the eCO_2RR activity and selectivity on Au catalyst in various electrolytes with different anions, including bicarbonate, perchlorate, sulfate, chloride, and carboxylates. For cation, salt of potassium were chosen due to its eCO_2RR-promoting role.[16, 18] We selected acetate (CH_3COO^-), propionate ($C_2H_5COO^-$), formate ($HCOO^-$), and trifluoroacetate (CF_3COO^-) as representative carboxylate anions for their structural closeness to bicarbonate. Because testing configuration (e.g. mass transfer of electrolytes) can affect absolute values of eCO_2RR activity and selectivity,[14, 32-34] we also performed eCO_2RR studies in presence of previously reported perchlorate, sulfate, and chloride anions to generate systematic 1-to-1 comparison across wide range of anions.[28, 35, 36] Specifically, to gain real-time insights into both reaction kinetics and overall reaction selectivity,[20, 32] we employed *in situ* Differential Electrochemical Mass Spectrometry (DEMS) approach for *operando* monitoring of products during eCO_2RR. Using *in situ* DEMS, we obtained production rates of both H_2 and CO molecules on Au catalyst surface as a function of potentials and selected anions.

RESULTS AND DISCUSSIONS

Anion Effect: Non-carboxylate anions case

First, we evaluated the anion effect on HER kinetics of polycrystalline Au using rotating-disk electrode (RDE) measurements for 3 different inorganic anions (i.e., perchlorate, sulfate and chloride) and benchmarked them against bicarbonate. In all cases, potassium (K^+) cation concentration was fixed at 0.1 M.[16, 18] Similar HER current densities were observed for all anions, except bicarbonate for which much larger HER activity was observed (**Figure 1a**). This result correlates well with prior reports by Resasco et al.[35] and Marcandalli et. Al.[14] which demonstrate that presence of bicarbonate promotes HER. High HER current in bicarbonate electrolyte can be rationalized by its lower pK_a value ($pK_{a,HCO3-}$ = 10.3 and $pK_{a,H2O}$ = 14) and therefore a more favorable proton-donating

ability of bicarbonate anion compared to water molecules. We further corroborated bicarbonate-driven HER by performing additional experiments in perchlorate-bicarbonate mixtures at different ratios, while maintaining [K^+] = 0.1 M (**Figure 1b**). Upon increase in bicarbonate molar fraction, lower HER overpotentials and thereby higher HER activities were observed (**Figure 1c**).

Next, we investigated anion effect for eCO_2RR activity and selectivity in the same set of electrolytes. Using *in situ* DEMS analysis, we quantified the respective CO_2RR and HER contributions (i.e., partial current density) to the observed total current density in CO_2-saturated electrolytes (**Figure S1-9**; See Experimental Section for details). CO is found to be a single major eCO_2RR product (**Figure S7**). We found that HER activity trend was similar to the Ar-saturated electrolytes case: HER currents were notably higher in bicarbonate electrolyte compared to the other anions (**Figure 1d**). Concurrently, eCO_2RR-to-CO conversion is characterized by earlier onset potential in bicarbonate (E_{onset} = -0.30 V vs. RHE) than other anions (E_{onset} ≈ -0.5 V vs. RHE) (**Figure 1e**), indicating a more favorable eCO_2RR kinetics in presence of bicarbonate compared to perchlorate, sulfate, and chloride electrolytes. Beneficial role of bicarbonate can be also observed when eCO_2RR activity is compared in SHE-scale (**Figure S10**). This result can be rationalized by the an increase in the transient CO_2 concentration near the catalyst surface through formation of the complex as suggested by Dunwell et al.[23] and Zhu et al.[24] Meanwhile, we observe negligible differences in eCO_2RR and HER activities for perchlorate, sulfate, and chloride.

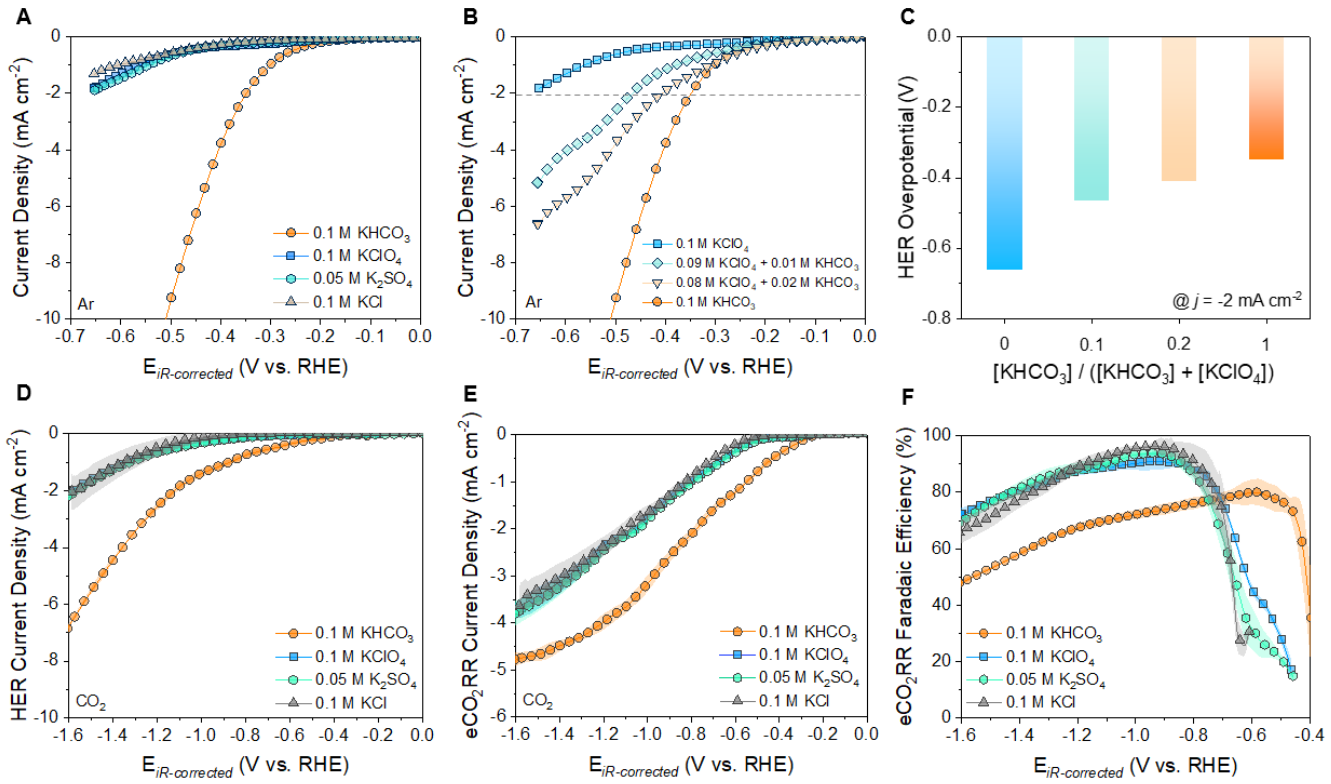

FIGURE 1. (A, B) Linear sweep voltammetry for HER activity on polycrystalline Au catalyst in Ar-saturated K^+-based electrolytes: (A) Bicarbonate, perchlorate, sulfate, and chloride anions, and (B) Mixture of bicarbonate and perchlorate anions (Scan rate = 5 mV s^{-1}, rotation speed = 3000 rpm) (C) HER overpotential at current density j=-2 mA cm^{-2}. (D) HER and I eCO_2RR partial current density on Au thin-film catalyst in CO_2-saturated electrolytes. (Scan rate = 5 mV s^{-1}, flow rate = 60 mL min^{-1}) (F) Faradaic efficiency for eCO_2RR in each carboxylate electrolytes. The translucent area represents error bar at each potential calculated from the standard deviation of three individual measurements.

Finally, we compared Faradaic efficiency (FE) for CO_2-to-CO conversion as a function of applied potential and anion type (**Figure 1f**). Bicarbonate features the well-known bell curve where its peak value of 80% appears at -0.6 V (vs. RHE), corresponding to previous reports.[33, 37, 38] More specifically, FE rapidly increases with beginning of CO evolution (from E = -0.4 V vs. RHE), peaks at around 80% (E = -0.6 V vs. RHE), decreases due to much faster HER increase (E < -0.6 V vs. RHE), and further decreases rapidly because of both mass transfer-limited eCO_2RR and exponential increase in water-splitting HER (E < -1.2 V vs. RHE). Although non-bicarbonate anions are characterized by much lower HER partial current densities compared to bicarbonate, they suffer from lower selectivity at > -0.8 V (vs. RHE) due to poor eCO_2RR kinetics. However, at the potentials below CO evolution onset of E ≈ -0.5 V (vs. RHE), FE value increases rapidly, reaching peak values >90%. This is notably higher than in bicarbonate case (**Figure 1f**). For all electrolytes, once the FE peak is reached, the selectivity decreases for more negative potential due to an increased contribution of HER from water molecules. These results show that while bicarbonate promotes eCO_2RR and hence larger overall CO production rates, its presence can negatively affect product selectivity since it concurrently promotes HER due to relatively facile bicarbonate-driven HER kinetics. In contrast, while anions like perchlorate, sulfate, and chloride can enable high FE of CO-production, they are characterized by less favorable eCO_2RR kinetics.

Anion Effect: Carboxylate anions case

Carboxylate anions display structural similarity to bicarbonate anion with negatively charged carboxyl group. Therefore, they can potentially participate in stabilization of CO_2RR intermediates yet so far there had been almost no reports studying carboxylate-based electrolytes for eCO_2RR. Herein, we studied eCO_2RR activity and selectivity in acetate, propionate, formate, and trifluoroacetate. Each of these anions displays a different electron density on the carboxylic acid group and thereby is characterized by distinct pK_a values (**Table S1).**

First, we analyzed HER activity in Ar-saturated electrolytes. All carboxylate anions display delayed HER onset potential compared to bicarbonate, similar to the case of perchlorate, sulfate, and chloride (**Figure 2a**). This is due to the favorable proton-donation ability of bicarbonate compared to water that leads to bicarbonate-driven HER kinetics in addition to water-driven HER.[14, 35]

On the other hand, additional HER partial currents emerge at potentials between -0.1 and -0.7 V (vs. RHE) in carboxylate-based electrolytes (*in situ* DEMS results: **Figure 2b**) when electrolytes are saturated with CO_2 causing the pH drop (**Table S2**). Considering the pH value of CO_2-saturated electrolytes and pK_b value of these anions (**Table S1**), those additional HER currents can be attributed to HER from conjugate acids (e.g. CH_3COOH or C_2H_5COOH) since their equilibrium concentration becomes non-negligible at lower pH (i.e. pH after CO_2 saturation, **Table S2**). For instance, 8.4 mM of CH_3COOH is estimated to be present as conjugate acid in CO_2-saturated 0.1 M CH_3COOK electrolyte (pH=5.8, pK_a=4.75). When the pH of Ar-saturated 0.1 M CH_3COOK is adjusted to 5.8 by adding 8.4 mM CH_3COOH, HER activity on Au surface exhibits the same early evolution of HER current at E = -0.1 V (vs. RHE) as **Figure 2b** (**Figure S11**). However, upon further potential decrease, the HER current density decreases before reaching its minimum (e.g., at E=-0.8 V (vs. RHE) for propionate). We assume that this is a result of the local pH increase that leads to chemical equilibrium shift and thereby decrease of conjugate acid concentration within the diffusion layer. Similar assumptions are valid for the propionate case. This HER feature is nearly absent in formate and completely disappears in trifluoroacetate electrolytes due to negligible concentration of conjugate acid molecules is expected due to their higher pK_b (**Table S1**).

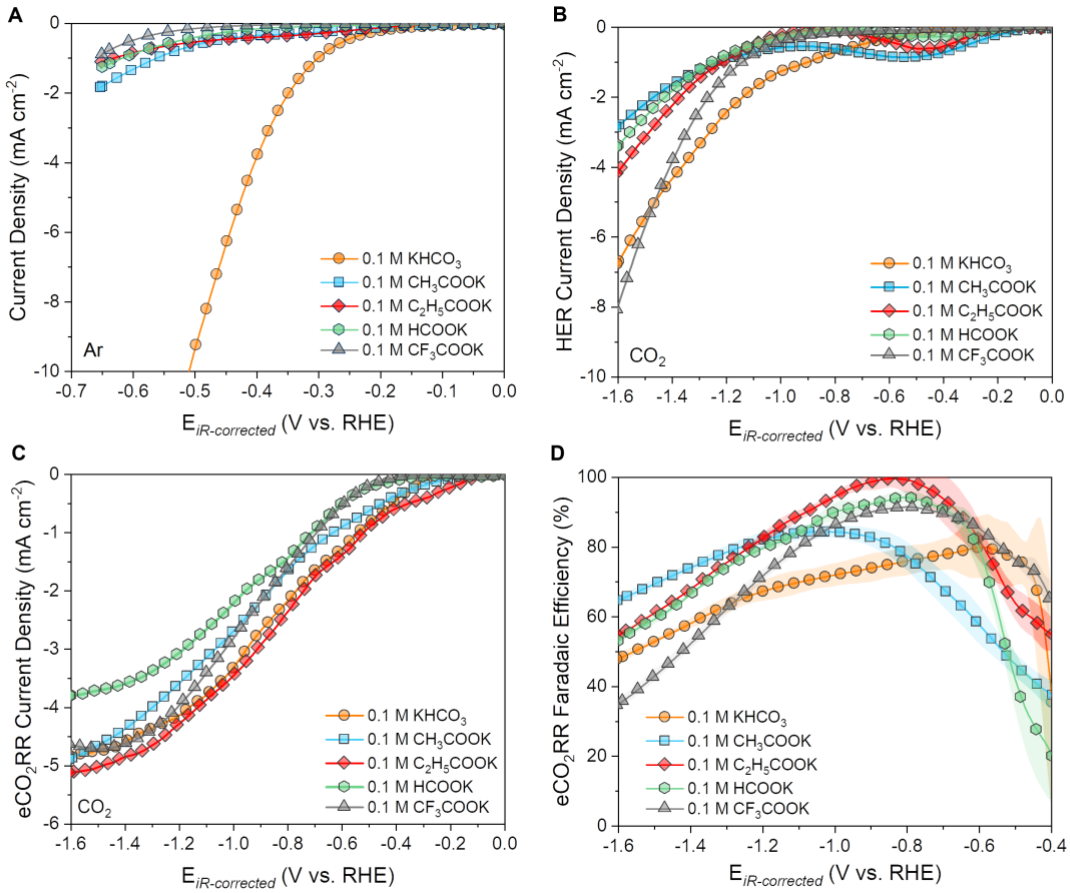

FIGURE 2**.** (A) HER activity of polycrystalline Au electrode using rotating-disk electrode (Scan rate = 5 mV s^{-1}, rotation speed = 3000 rpm). (B) HER and (C) eCO_2RR partial current density on Au thin-film catalyst in CO_2-saturated electrolytes. (Scan rate = 5 mV s^{-1}, flow rate = 60 mL min^{-1}) (D) Faradaic efficiency for eCO_2RR in each carboxylate electrolytes. The translucent area represents error bar at each potential calculated from the standard deviation of three individual measurements.

Next, we analyzed effect of carboxylate anions on eCO_2RR partial currents and CO evolution onsets (**Figure 2c**). In contrast to non-carboxylate anions that are characterized by more sluggish eCO_2RR kinetics and later CO-evolution onsets (E = -0.5 V vs RHE), both acetate and propionate anions reveal an early eCO_2RR onset potential at E = -0.2 V (vs. RHE) and eCO_2RR current density closely comparable to bicarbonate electrolytes. Meanwhile, eCO_2RR in formate and trifluoroacetate electrolytes is characterized by the higher overpotentials compared to bicarbonate (**Table S3**).

Finally, we plotted anion-specific FE (eCO_2RR) trends as a function of applied potential (**Figure 2d**). At low overpotential range (i.e., E = -0.4 ~-0.6 V vs. RHE), that is characterized by low overall current densities (**Figure S12**), a lower faradaic efficiency towards CO is observed for acetate and propionate anions than bicarbonate due to larger acid-driven HER currents compared to eCO_2RR. Meanwhile, for the intermediate potential range (i.e., E < -0.6 V vs. RHE), much higher FE values can be achieved in all carboxylate electrolytes compared to bicarbonate due to bicarbonate-driven HER and a decrease of conjugate carboxylate acid-driven HER contributions. The highest

eCO_2RR selectivity is observed at E = -0.8 V (vs. RHE), where acid-driven HER is minimized and water-driven HER is not yet initiated. Here, the highest FE is observed for propionate, reaching an exceptional FE value of 99.6% (±2.6%), and slightly lower FE are reached for formate (94.2±1.7%) and trifluoroacetate (91.5±0.5%) electrolytes due to more sluggish eCO_2RR kinetics in these electrolytes. The lowest FE (84±1.0%) is reached in acetate electrolytes due to significant contribution of acid-driven HER (**Figure 2b**). Hence, presence of specific carboxylate anions can enable significantly higher eCO_2RR selectivity compared to bicarbonate which can be particularly promising for higher current density conditions.

We summarize the observed anion-dependent HER and eCO_2RR schematically in Figure 3. While bicarbonate is highly beneficial for eCO_2RR activity, at the same time it promotes HER (from bicarbonate) decreasing overall eCO_2RR selectivity at higher currents/overpotentials (E < -0.6 V vs. RHE). When bicarbonate anion is replaced by either perchlorate, sulfate, or chloride, HER current is largely suppressed, leading to much higher eCO_2RR Faradaic efficiency at potentials below E = -0.8 V (vs. RHE). Yet, the absence of bicarbonate also leads to substantial decrease in eCO_2RR activity (i.e., CO partial currents) in these electrolytes. Finally, a separate case represents carboxylate anions: overall, HER is largely suppressed by excluding bicarbonate-related HER reduction, while eCO_2RR activity and selectivity varies depending on the carboxylate type, reaching the maximum in the case of propionate. As a result, both high eCO_2RR activity and selectivity was achieved together in 0.1 M C_2H_5COOK electrolyte, overcoming limitations characteristic of electrolytes with bicarbonate or salts of conventional inorganic anions.

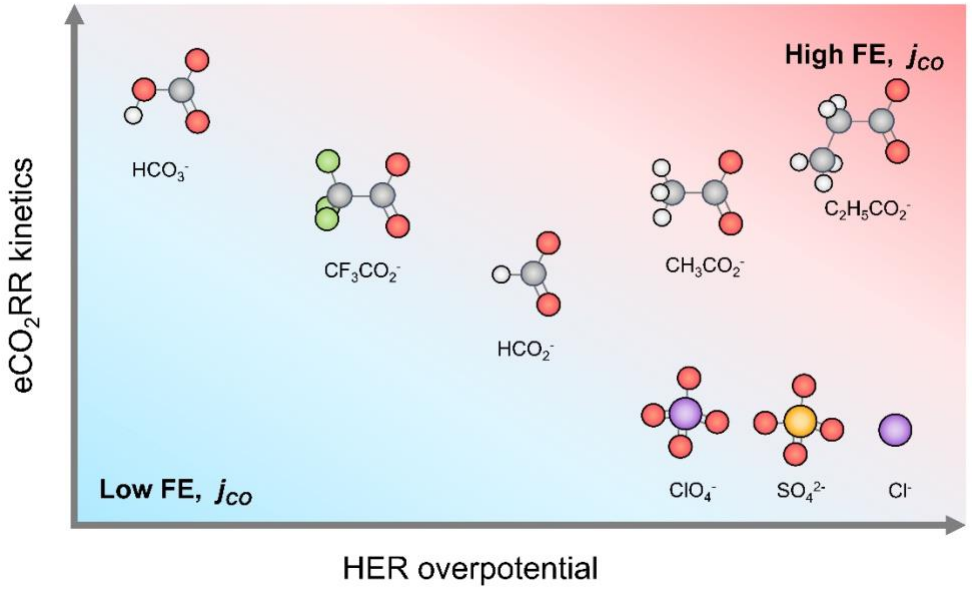

FIGURE 3. Schematic illustration of different anion effect on HER and eCO_2RR activity depending on molecular structures.

CONCLUSIONS

In summary, we used real-time monitoring to study the effects of different anions on the evolution of H_2 and CO molecules during electrochemical CO_2 conversion. First, we show that when electrolytes with inorganic anions such as perchlorate, sulfate, and chloride were used instead of bicarbonate they show similar impact of eCO_2RR: while they suppress HER (due to absence of bicarbonate-driven HER), for all an increased eCO_2RR overpotentials

and decreased CO production rates are observed. Next, carboxylate anions with different molecular structures were explored. We found that specific carboxylate electrolytes promote a more favorable CO_2 reduction kinetics compared to inorganic anions, with propionate anion promoting the highest eCO_2RR activity. Due to their reduced H_2 evolution activity compared to bicarbonate, carboxylate anions offer significantly higher CO_2 reduction selectivity, with the peak Faradaic efficiency values as follows: acetate (84%) < trifluoroacetate (91%) < formate (94%) < propionate (99%). In conclusion, this study emphasizes the crucial role of anions in controlling HER and maximizing CO_2 reduction in electrolyte engineering for advanced electrochemical CO_2 conversion systems.

ASSOCIATED CONTENT

Supporting Information. The Supporting Information is available free of charge at http://pubs.acs.org."

Experimental data (PDF)

AUTHOR INFORMATION

Corresponding Author

Maria R. Lukatskaya* – Department of Mechanical and Process Engineering, ETH Zurich, 8092 Zurich, Switzerland; E-mail: mlukatskaya@ethz.ch

Author

Ji Mun Yoo – Department of Mechanical and Process Engineering, ETH Zurich, 8092 Zurich, Switzerland

Author Contributions

The manuscript was written through contributions of all authors. All authors have given approval to the final version of the manuscript.

Notes

The authors declare no competing financial interest.

ACKNOWLEDGMENT

M.R.L. acknowledge support from the ETH Foundation. J.M.Y. gratefully acknowledges Schmidt Science Fellowship funded by Schmidt Futures in partnership with the Rhodes Trust (Oxford, United Kingdom).

EXPERIMENTAL METHODS

2.1 Chemicals. Electrolytes were prepared from $KHCO_3$ (99.7%, Sigma-Aldrich), CH_3COOK (≥99.0%, Sigma-Aldrich), C_2H_5COOK (≥98%, TCI), HCOOK (99.9%, Sigma-Aldrich), CF_3COOK (≥98%, TCI), $KClO_4$ (≥99%, Sigma-Aldrich), K_2SO_4 (≥99%, Sigma-Aldrich), KCl (99.5%, Sigma-Aldrich), and Ultrapure water (Milli-Q grade, ≥18.2 MΩcm, ACCU 20, Scientific Fisher). H_2SO_4 (95.0-98.0%, ACS reagent, Sigma-Aldrich) is used for electrochemical cell cleaning. Ar (5.0 purity, PanGas) and CO_2(4.5 purity, PanGas) were used for purging electrolytes.

2.2 Electrolyte purification. To remove metallic impurities, each electrolyte was electrochemically purified by applying current density of 0.1 mA cm^{-2} between two Au electrodes for 12 hours.[20, 39] HCOOK electrolytes were used without electrochemical purification to prevent formate oxidation reactions on anode side.

2.3 Electrochemical measurements. All electrochemical measurements were conducted using VSP-300 potentiostat (Biologic) equipped with EC-LAB software. Onset potential of HER and eCO_2RR is defined as potential value at -0.1 mA cm^{-2} of partial current density in this work because it corresponds to DEMS detection limit

threshold. For each experiment, *iR* correction is applied at 85% compensation of uncompensated resistance measured by electrochemical impedance spectroscopy. Three independent experiments were conducted for each electrolyte for calculation of error bar. All electrochemical potentials were converted from Ag/AgCl scale to RHE using the following equation:

$$E_{RHE} = E_{Ag/AgCl} + 0.059 \times pH_{Bulk} + 0.205$$

2.3 RDE experiment. RDE experiment was conducted in H-type glass cell in 3-electrode configuration using RRDE-3A equipment (ALS). Polycrystalline Au disk (ALS) was used as working electrode. Leakless Ag/AgCl electrode (eDAQ, 3.4 M KCl) and large area graphite rod were used as reference and counter electrodes, respectively. Nafion 211 membrane (Sigma-Alrich) was used to separate catholyte and anolyte to avoid product cross-over. Before RDE experiment, the Nafion membrane was cation-exchanged by immersing in 0.1 M NaOH and rinsed with copious amounts of DI water.

Prior to each experiment, the glass cell was cleaned by immersing in 0.05 M H_2SO_4 solution for 1 hour, followed by boiling in DI water for 10 min which is repeated two times. Au electrode was polished with 0.3 µm and 0.05 µm alumina powders (CH Instrument) sequentially, and ultrasonicated in 1:1 mixture of DI water and 2-isopropanol for 10 min to ensure removal of polishing alumina powder. Then polished Au electrode was mounted on rotator (RRDE-3A, ALS), and immersed into electrolyte. Before start of electrochemical experiment, each electrolyte was pre-bubbled by Ar for at least 20 min. Then, linear sweep voltammetry is conducted to measure HER kinetics on Au surface (scan rate of 5 mV s^{-1} at 3000 rpm rotation speeds). For each measurement, *iR* correction was applied at 85% compensation of uncompensated resistance values measured by electrochemical impedance spectroscopy.

2.4 Preparation of Au electrode for DEMS measurement. Nanoporous PTFE membrane (20 nm of pore size, Cobetter Filtration Equipment) was used as both pervaporation membrane for DEMS and substrate for Au electrocatalyst. Before Au deposition, the PTFE membrane was sonicated in ethanol for 30 min. 400 nm of Au thin film was deposited on the PTFE membrane for optimal product molecule detection[32] using electron-beam physical vapor deposition (Creamet 450 e-beam). Polycrystalline structure of the deposited Au thin film was confirmed using X-ray diffraction (XRD) (Figure S1).

2.5 Electrochemical flow cell for *in situ* DEMs. *in situ* DEMS experiment was conducted using 2 compartment homemade 3-electrode PEEK flow cell (design similar to previous literature[32]). Au-deposited nanoporous PTFE membrane served as a working electrode, Pt mesh served as a counter electrode and leakless Ag/AgCl (eDAQ) as a reference. Cation-exchanged Nafion membrane was used to separate cathode and anode compartments.

Before each experiment, the cell was thoroughly cleaned by soaking in 0.05 M H_2SO_4 solution for 1 h, followed by boiling in DI water for 10 min which is repeated two times. Each electrode chamber was pumped with electrolytes using peristaltic pump (Baoding Shenchen Precision pump) at flow rate of 60 mL min^{-1}. Catholyte and anolyte were pumped from/into separated electrolyte reservoirs to prevent species cross-over from anode to cathode during experiments.

2.5 *in situ* DEMS experiment. Electrochemical measurements were carried out using Biologic VSP-300 potentiostat. Electrochemical surface area (ECSA) of the Au thin film working electrode is calculated by dividing reduction charge of Au oxide during cyclic voltammetry in 0.05 M H_2SO_4 by specific reduction charge of Au oxide monolayer on polycrystalline Au (390 µC cm_{Au}^{-2}) (Figure S2).[40] This value is used for calculating ECSA-normalized current density. Before each experiment, electrolytes were saturated by Ar or CO_2 for at least 20 min prior being

pumped into the flow cell, for HER or eCO_2RR measurements, respectively. Next, Au thin film electrode (on PTFE membrane) was conditioned in each electrolyte by conducting cyclic voltammetry between 0.4 and 1.7 V (vs. RHE) at scan rate of 50 mV s^{-1} for 3 cycles. Then, linear sweep voltammetry (LSV) was conducted at scan rate of 5 mV s^{-1} for both HER and eCO_2RR measurements. During LSV, mass spectra were acquired by HPR40 mass spectrometer (Hiden Analytic) at 70 eV of electron energy and 500 µA of emission current. Secondary electron multiplier detector was used at voltage of 1350 V.

For quantitative product analysis a calibration of H_2 and CO across Au-deposited nanoporous PTFE membrane was conducted by applying a modified methodology from literature.[32] Briefly, H_2 calibration was conducted *in situ* by directly comparing HER current from LSV and H_2 signal (m/z=2) at each potential in Ar-saturated $KHCO_3$ electrolyte (Figure S3). Then, HER current density was plotted against m/z=2 mass-ion signal and using linear fitting, H_2 calibration was generated and later on used to convert the measured m/z=2 mass-ion signal to HER current density (Figure S4). The accuracy of H_2 calibration was confirmed by observing an overlap between HER current directly measured from potentiostat and HER current calculated from DEMS m/z=2 signal using calibration curve (Figure S5). Next, CO signal calibration was conducted by measuring m/z=2, 28, and 44 mass-ion signals together. Using the H_2 calibration results, eCO_2RR partial current were obtained by calculating HER partial current first and then subtracting its contribution from the total current (Figure S6). Then, produced net CO signal was calculated by subtracting the fragmental signal of CO_2 (m/z=44) to m/z=28, which is denoted as m/z(CO)=28. By plotting m/z(CO)=28 against eCO_2RR partial current, a linear CO calibration line fitting was obtained (Figure S7), indicating that CO is the dominant eCO_2RR product on Au surface (in agreement with prior studies).[10, 37] Based on these calibrations, Faradaic efficiency (FE) of eCO_2RR was calculated (Figure S8).

REFERENCES

1. Nielsen, D. U.; Hu, X.-M.; Daasbjerg, K.; Skrydstrup, T., Chemically and electrochemically catalysed conversion of CO2 to CO with follow-up utilization to value-added chemicals. *Nat. Catal.* **2018,** *1* (4), 244-254.
2. Shafaat, H. S.; Yang, J. Y., Uniting biological and chemical strategies for selective CO2 reduction. *Nat. Catal.* **2021,** *4* (11), 928-933.
3. Nitopi, S.; Bertheussen, E.; Scott, S. B.; Liu, X.; Engstfeld, A. K.; Horch, S.; Seger, B.; Stephens, I. E. L.; Chan, K.; Hahn, C.; Nørskov, J. K.; Jaramillo, T. F.; Chorkendorff, I., Progress and Perspectives of Electrochemical CO2 Reduction on Copper in Aqueous Electrolyte. *Chem. Rev.* **2019,** *119* (12), 7610-7672.
4. Birdja, Y. Y.; Pérez-Gallent, E.; Figueiredo, M. C.; Göttle, A. J.; Calle-Vallejo, F.; Koper, M. T. M., Advances and challenges in understanding the electrocatalytic conversion of carbon dioxide to fuels. *Nat. Energy* **2019,** *4* (9), 732-745.
5. Gao, D.; Arán-Ais, R. M.; Jeon, H. S.; Roldan Cuenya, B., Rational catalyst and electrolyte design for CO2 electroreduction towards multicarbon products. *Nat. Catal.* **2019,** *2* (3), 198-210.
6. Wagner, A.; Sahm, C. D.; Reisner, E., Towards molecular understanding of local chemical environment effects in electro- and photocatalytic CO2 reduction. *Nat. Catal.* **2020,** *3* (10), 775-786.
7. Bui, J. C.; Kim, C.; King, A. J.; Romiluyi, O.; Kusoglu, A.; Weber, A. Z.; Bell, A. T., Engineering Catalyst-Electrolyte Microenvironments to Optimize the Activity and Selectivity for the Electrochemical Reduction of CO(2) on Cu and Ag. *Acc. Chem. Res.* **2022,** *55* (4), 484-494.
8. Marcandalli, G.; Monteiro, M. C. O.; Goyal, A.; Koper, M. T. M., Electrolyte Effects on CO(2) Electrochemical Reduction to CO. *Acc. Chem. Res.* **2022,** *55* (14), 1900-1911.
9. Xu, A.; Govindarajan, N.; Kastlunger, G.; Vijay, S.; Chan, K., Theories for Electrolyte Effects in CO(2) Electroreduction. *Acc. Chem. Res.* **2022,** *55* (4), 495-503.

10. Ringe, S.; Morales-Guio, C. G.; Chen, L. D.; Fields, M.; Jaramillo, T. F.; Hahn, C.; Chan, K., Double layer charging driven carbon dioxide adsorption limits the rate of electrochemical carbon dioxide reduction on Gold. *Nat. Commun.* **2020,** *11* (1), 33.
11. Wuttig, A.; Yaguchi, M.; Motobayashi, K.; Osawa, M.; Surendranath, Y., Inhibited proton transfer enhances Au-catalyzed CO2-to-fuels selectivity. *Proc. Natl. Acad. Sci. U. S. A.* **2016,** *113* (32), E4585-93.
12. Gill, T. M.; Furst, A. L., Interfacial electrolyte effects on aqueous CO2 reduction: Learning from enzymes to develop inorganic approaches. *Curr. Opin. Electrochem.* **2022,** *35*.
13. Konig, M.; Vaes, J.; Klemm, E.; Pant, D., Solvents and Supporting Electrolytes in the Electrocatalytic Reduction of CO(2). *iScience* **2019,** *19*, 135-160.
14. Marcandalli, G.; Goyal, A.; Koper, M. T. M., Electrolyte Effects on the Faradaic Efficiency of CO(2) Reduction to CO on a Gold Electrode. *ACS Catal.* **2021,** *11* (9), 4936-4945.
15. Banerjee, S.; Gerke, C. S.; Thoi, V. S., Guiding CO(2)RR Selectivity by Compositional Tuning in the Electrochemical Double Layer. *Acc Chem Res* **2022,** *55* (4), 504-515.
16. Monteiro, M. C. O.; Dattila, F.; Hagedoorn, B.; García-Muelas, R.; López, N.; Koper, M. T. M., Absence of CO2 electroreduction on copper, gold and silver electrodes without metal cations in solution. *Nat. Catal.* **2021,** *4* (8), 654-662.
17. Singh, M. R.; Kwon, Y.; Lum, Y.; Ager, J. W., III; Bell, A. T., Hydrolysis of Electrolyte Cations Enhances the Electrochemical Reduction of CO2 over Ag and Cu. *J. Am. Chem. Soc.* **2016,** *138* (39), 13006-13012.
18. Resasco, J.; Chen, L. D.; Clark, E.; Tsai, C.; Hahn, C.; Jaramillo, T. F.; Chan, K.; Bell, A. T., Promoter Effects of Alkali Metal Cations on the Electrochemical Reduction of Carbon Dioxide. *J. Am. Chem. Soc.* **2017,** *139* (32), 11277-11287.
19. Monteiro, M. C. O.; Dattila, F.; López, N.; Koper, M. T. M., The Role of Cation Acidity on the Competition between Hydrogen Evolution and CO2 Reduction on Gold Electrodes. *J. Am. Chem. Soc.* **2022,** *144* (4), 1589-1602.
20. Ye, K.; Zhang, G.; Ma, X.-Y.; Deng, C.; Huang, X.; Yuan, C.; Meng, G.; Cai, W.-B.; Jiang, K., Resolving local reaction environment toward an optimized CO2-to-CO conversion performance. *Energy & Environ. Sci.* **2022,** *15* (2), 749-759.
21. Gu, J.; Liu, S.; Ni, W.; Ren, W.; Haussener, S.; Hu, X., Modulating electric field distribution by alkali cations for CO2 electroreduction in strongly acidic medium. *Nat. Catal.* **2022,** *5* (4), 268-276.
22. Qin, X.; Vegge, T.; Hansen, H. A., Cation-Coordinated Inner-Sphere CO(2) Electroreduction at Au-Water Interfaces. *J. Am. Chem. Soc.* **2023,** *145* (3), 1897-1905.
23. Dunwell, M.; Lu, Q.; Heyes, J. M.; Rosen, J.; Chen, J. G.; Yan, Y.; Jiao, F.; Xu, B., The Central Role of Bicarbonate in the Electrochemical Reduction of Carbon Dioxide on Gold. *J. Am. Chem. Soc.* **2017,** *139* (10), 3774-3783.
24. Zhu, S.; Jiang, B.; Cai, W. B.; Shao, M., Direct Observation on Reaction Intermediates and the Role of Bicarbonate Anions in CO(2) Electrochemical Reduction Reaction on Cu Surfaces. *J. Am. Chem. Soc.* **2017,** *139* (44), 15664-15667.
25. Shan, W.; Liu, R.; Zhao, H.; Liu, J., Bicarbonate Rebalances the *COOH/*OCO(-) Dual Pathways in CO(2) Electrocatalytic Reduction: In Situ Surface-Enhanced Raman Spectroscopic Evidence. *J. Phys. Chem. Lett.* **2022,** *13* (31), 7296-7305.
26. Wuttig, A.; Yoon, Y.; Ryu, J.; Surendranath, Y., Bicarbonate Is Not a General Acid in Au-Catalyzed CO(2) Electroreduction. *J. Am. Chem. Soc.* **2017,** *139* (47), 17109-17113.
27. Varela, A. S.; Ju, W.; Reier, T.; Strasser, P., Tuning the Catalytic Activity and Selectivity of Cu for CO2 Electroreduction in the Presence of Halides. *ACS Catal.* **2016,** *6* (4), 2136-2144.
28. Ovalle, V. J.; Waegele, M. M., Impact of Electrolyte Anions on the Adsorption of CO on Cu Electrodes. *J. Phys. Chem. C* **2020,** *124* (27), 14713-14721.
29. Yuan, T.; Wang, T.; Zhang, G.; Deng, W.; Cheng, D.; Gao, H.; Zhao, J.; Yu, J.; Zhang, P.; Gong, J., The effect of specific adsorption of halide ions on electrochemical CO(2) reduction. *Chem. Sci.* **2022,** *13* (27), 8117-8123.

30. Gao, D.; McCrum, I. T.; Deo, S.; Choi, Y.-W.; Scholten, F.; Wan, W.; Chen, J. G.; Janik, M. J.; Roldan Cuenya, B., Activity and Selectivity Control in CO2 Electroreduction to Multicarbon Products over CuOx Catalysts via Electrolyte Design. *ACS Catal.* **2018,** *8* (11), 10012-10020.
31. Gao, D.; Scholten, F.; Roldan Cuenya, B., Improved CO2 Electroreduction Performance on Plasma-Activated Cu Catalysts via Electrolyte Design: Halide Effect. *ACS Catal.* **2017,** *7* (8), 5112-5120.
32. Clark, E. L.; Bell, A. T., Direct Observation of the Local Reaction Environment during the Electrochemical Reduction of CO(2). *J. Am. Chem. Soc.* **2018,** *140* (22), 7012-7020.
33. Goyal, A.; Marcandalli, G.; Mints, V. A.; Koper, M. T. M., Competition between CO(2) Reduction and Hydrogen Evolution on a Gold Electrode under Well-Defined Mass Transport Conditions. *J. Am. Chem. Soc.* **2020,** *142* (9), 4154-4161.
34. Watkins, N. B.; Schiffer, Z. J.; Lai, Y.; Musgrave, C. B., III; Atwater, H. A.; Goddard, W. A., III; Agapie, T.; Peters, J. C.; Gregoire, J. M., Hydrodynamics Change Tafel Slopes in Electrochemical CO2 Reduction on Copper. *ACS Energy Lett.* **2023,** *8* (5), 2185-2192.
35. Resasco, J.; Lum, Y.; Clark, E.; Zeledon, J. Z.; Bell, A. T., Effects of Anion Identity and Concentration on Electrochemical Reduction of CO2. *ChemElectroChem* **2018,** *5* (7), 1064-1072.
36. Hashiba, H.; Weng, L.-C.; Chen, Y.; Sato, H. K.; Yotsuhashi, S.; Xiang, C.; Weber, A. Z., Effects of Electrolyte Buffer Capacity on Surface Reactant Species and the Reaction Rate of CO2 in Electrochemical CO2 Reduction. *J. Phys. Chem. C* **2018,** *122* (7), 3719-3726.
37. Hori, Y.; Murata, A.; Kikuchi, K.; Suzuki, S., Electrochemical reduction of carbon dioxides to carbon monoxide at a gold electrode in aqueous potassium hydrogen carbonate. *Journal of the Chemical Society, Chemical Communications* **1987,** (10), 728-729.
38. Cave, E. R.; Montoya, J. H.; Kuhl, K. P.; Abram, D. N.; Hatsukade, T.; Shi, C.; Hahn, C.; Nørskov, J. K.; Jaramillo, T. F., Electrochemical CO2 reduction on Au surfaces: mechanistic aspects regarding the formation of major and minor products. *Physical Chemistry Chemical Physics* **2017,** *19* (24), 15856-15863.
39. Wuttig, A.; Surendranath, Y., Impurity Ion Complexation Enhances Carbon Dioxide Reduction Catalysis. *ACS Catalysis* **2015,** *5* (7), 4479-4484.
40. Łukaszewski, M. S., M.; Czerwinski, A., Electrochemical Methods of Real Surface Area Determination of Noble Metal Electrodes – an Overview. *Int. J. Electrochem. Sci.* **2016,** *11*, 4442-4469.